AGU PUBLICATIONS

JGR

Journal of Geophysical Research: Atmospheres

RESEARCH ARTICLE
10.1002/2013JD020610

Key Points:
- An XBT/GPS sonde observation was conducted across the Kuroshio front
- Local weakening of surface winds was found just above the Kuroshio front
- The weakening occurs at the onset of cross-frontal winds transiently

Correspondence to:
K. Kasamo,
kasamo@mepl1.cmes.ehime-u.ac.jp

Citation:
Kasamo, K., A. Isobe, S. Minobe, A. Manda, H. Nakamura, K. Ogata, H. Nishikawa, Y. Tachibana, and S. Kako (2014), Transient and local weakening of surface winds observed above the Kuroshio front in the winter East China Sea, *J. Geophys. Res. Atmos.*, *119*, 1277–1291, doi:10.1002/2013JD020610.

Received 13 AUG 2013
Accepted 8 JAN 2014
Accepted article online 13 JAN 2014
Published online 13 FEB 2014

Transient and local weakening of surface winds observed above the Kuroshio front in the winter East China Sea

Kenki Kasamo[1], Atsuhiko Isobe[1], Shoshiro Minobe[2], Atsuyoshi Manda[3], Hirohiko Nakamura[4], Koto Ogata[5], Hatsumi Nishikawa[5], Yoshihiro Tachibana[5,6], and Shin'ichiro Kako[7]

[1]Center for Marine Environmental Studies, Ehime University, Matsuyama, Japan, [2]Department of Natural History Sciences, Graduate School of Science, Hokkaido University, Sapporo, Japan, [3]Graduate School of Fisheries Science and Environmental Studies, Nagasaki University, Nagasaki, Japan, [4]Faculty of Fisheries, Kagoshima University, Kagoshima, Japan, [5]Climate and Ecosystem Dynamics Division, Mie University, Tsu, Japan, [6]Research Institute for Global Change, Japan Agency for Marine-Earth Science and Technology, Yokosuka, Japan, [7]Faculty of Engineering, Kagoshima University, Kagoshima, Japan

Abstract To confirm whether surface winds strengthen above warm waters around oceanic fronts using in situ data, a field measurement was conducted using both expendable bathythermographs and Global Positioning System sondes released concurrently across the Kuroshio front in the East China Sea in December 2010. In contrast to previous studies mainly based on satellite observations, the finding of the present field survey is the local weakening of surface winds at the northern flank of the Kuroshio front. From the above field observation in conjunction with a regional numerical model experiment, it is suggested that the northwesterly winds crossing the Kuroshio front from the cooler side first weaken at the northern flank of the front because of the onset of upward transfer of the "nonslip" condition at the sea surface. Thereafter, as the atmospheric mixed layer with warm and humid air mass develops gradually downwind over the Kuroshio region, the surface winds are gradually accelerated by the momentum mixing with strong winds aloft. The surface winds remain strong over the cool East China Sea shelf, and it is thus considered that the surface winds only weaken at the northern flank of the Kuroshio front. However, numerical modeling indicates that this local weakening of the surface winds occurs as a transient state with a short duration and such a structure has thus rarely been detected in the long-term averaged wind fields observed by satellites.

1. Introduction

Recent satellite observations have revealed positive correlation between sea surface temperature (SST) and surface wind speeds, although there is debate whether wind speeds increase above warm currents because of the vertical momentum transfer in atmospheric boundary layers [*Wallace et al*., 1989] or because of an adjustment of the sea level pressure above oceanic fronts [*Lindzen and Nigam*, 1987]. For instance, in analyses of satellite-derived SST and wind data derived from both the Quick Scatterometer (QuikSCAT) and NASA Scatterometer (NSCAT), *Park et al*. [2006] found that there is a strong divergence (convergence) of surface winds on the upwind (downwind) side of warm-core rings of the Gulf Stream because of the destabilization of marine atmospheric boundary layers over high SST. In the case of the Kuroshio, using QuikSCAT and the joint US/Japan Tropical Rainfall Measuring Mission (TRMM/TRMM Microwave Imager (TMI)) data set, *Xie et al*. [2002] showed that intense winds prevail over the Kuroshio at the shelf break of the East China Sea during winter. *Pan et al*. [2002] also found atmospheric convergence zones along both the Gulf Stream and the Kuroshio, using QuikSCAT, NSCAT, and European Remote Sensing (ERS)-1/2 satellite data. In addition, *Minobe et al*. [2008] and *Takatama et al*. [2012] focused on the effects of the adjustment of the sea level pressure on the wind field over the Gulf Stream.

Besides the areas above western boundary currents, satellite observations have revealed positive correlation between SST and surface winds on relatively small spatial scale across various oceans. For instance, using the satellite observations made by both QuikSCAT and the TRMM Microwave Imager, *Liu et al*. [2000] revealed that there is a coupling between winds and SST due to buoyancy instability and mixing over the equatorial Pacific. Likewise, in the eastern tropical Pacific, *Chelton et al*. [2001] indicated that the wind stress divergence (curl) is related to the downwind (crosswind) component of the SST gradient. Similar to the case for the tropics, where there is an intense coupling of the atmosphere and the ocean, there is a close relationship

©2014. American Geophysical Union. All Rights Reserved.

between SST and surface winds at midlatitude and high latitude. For instance, *Nonaka and Xie* [2003] found an increase (decrease) in wind speed above warm (cold) SST anomalies over the Kuroshio Extension as well as the Kuroshio south of Japan. Moreover, in the Okhotsk Sea, *Tokinaga and Xie* [2009] found that surface winds become weak over tide-induced cold patches. In the Southern Ocean, *O'Neill et al.* [2003] found that spatial variations of surface winds are dependent on those of an SST front and that this coupling relation may provide important feedback to upper ocean processes around the SST front. Overall, the close relationship between SST and surface wind speed (and hence the divergence and curl of wind speed) was well demonstrated by *Chelton et al*. [2004], who mapped the wind stress curl and divergence around the world ocean using QuikSCAT data.

The wind intensification and its related modification of both the wind stress curl and divergence above oceanic fronts no doubt occur, as reported by the above studies using satellite observations, which are indeed capable of obtaining horizontal views of physical quantities in both the ocean and the atmosphere. However, satellites are unable to observe how atmospheric properties change vertically because of the development of mixed layers in the low-level atmosphere or because of deep convection that may extend to the upper troposphere [e.g., *Minobe et al*., 2008]. In addition, unless otherwise observed on the ocean, there is no way of knowing whether satellite-derived wind fields (~25 km resolution) can capture with certainty atmospheric responses over the relatively narrow oceanic fronts with horizontal widths of *O*(100) km for western boundary currents. Therefore, it is of particular interest to look over a vertical cross section on which atmospheric and oceanic properties (e.g., potential temperature) observed concurrently in the actual atmosphere and ocean are depicted together. How deep are oceanic influences on the atmosphere? Is the wind intensification above the Kuroshio, which certainly appears in the climatological wind fields, a "robust" response found even in a snapshot observation? Are there fine atmospheric structures unable to be observed by satellites around the relatively narrow oceanic fronts? In this study, vertical cross sections of both oceanic and atmospheric properties are obtained concurrently using either expendable bathythermographs (XBTs) or Global Positioning System (GPS) sondes during an observational cruise repeatedly crossing the Kuroshio front at the shelf break of the winter East China Sea. Thereafter, a relationship between atmospheric and oceanic properties found from the data obtained on this observational cruise is interpreted using a regional atmospheric circulation model.

2. Data and Method

2.1. XBT and GPS Sonde Observations

An observation in which both XBTs and GPS sondes were released simultaneously was conducted on-board the T/V *Nagasaki-maru*, belonging to the Faculty of Fisheries of Nagasaki University, during the period 2130 UTC on 2 December through 1800 UTC on 4 December (44.5 h in total) 2010. Figure 1 shows observation stations at which XBTs and GPS sondes were released concurrently once an hour during the four-time repeated surveys along the observation line. Some stations were skipped during the surveys because of the failure of the sonde release, and thus, XBT/sonde casts were conducted 37 times in total. Also shown are isotherms derived from the Reynolds SST data set (*Reynolds et al*., 2007; downloaded from http://www.ncdc.noaa.gov/oa/climate/research/sst/griddata.php) on 4 December 2010. It seems likely that the northern half of the observation line crossed the Kuroshio front between isotherms of 22.5°C and 23.5°C at 29.5°N–30°N. Although the Reynolds SST has horizontal resolution of 0.25° in both latitude and longitude, the location of the Kuroshio front is nearly the same as that determined by XBT surveys with an observation station interval of 1/6° in latitude (shown later in Figure 5). In this observation, the XBTs falling downward observed seawater temperature every 0.25 s from the surface to a depth of 750 m, while the balloon-equipped GPS sondes flying upward observed air temperature, wind vectors, and specific humidity once every second from the surface to a height of 200 hPa.

It is likely that relatively narrow (~100 km) oceanic fronts alter atmospheric processes with horizontal scales much smaller than the synoptic scale, and so spatiotemporal variations associated with the passage of extratropical cyclones and/or anticyclones should be removed from the GPS sonde data as much as possible. Figure 2 shows the sea level pressure maps over East Asia drawn using the National Centers for Environmental Prediction (NCEP) reanalysis data provided by the National Oceanic and Atmospheric Administration (http://www.esrl.noaa.gov/psd/data/gridded/data.ncep.reanalysis.surface.html). It is found that a high-pressure system gradually moved eastward above the observational area during the period 2–4 December, and it is thus reasonable to

©2014. American Geophysical Union. All Rights Reserved.

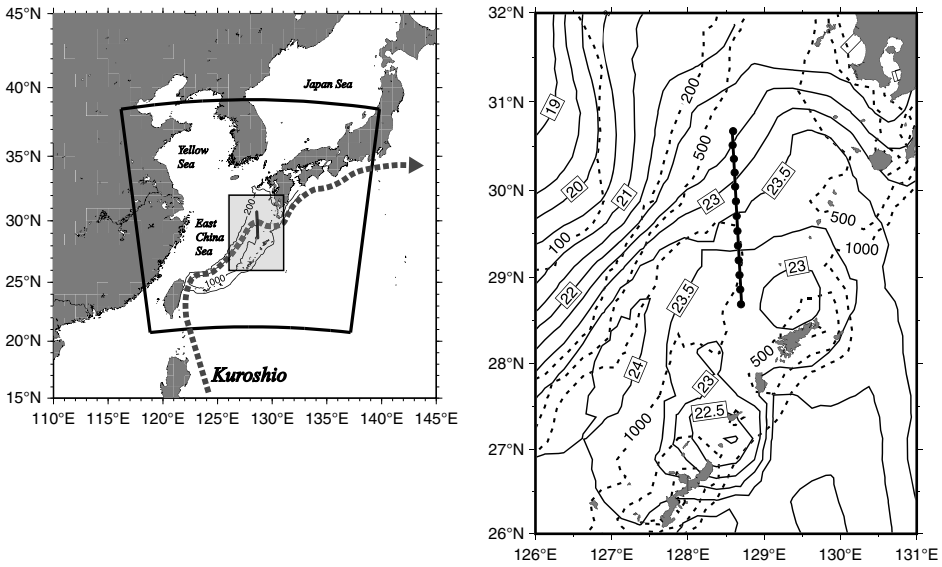

Figure 1. Study area and observation stations. (left) The broken curve with the arrow indicates the Kuroshio path schematically, and the solid lines show isobaths of 200 and 1000 m. The area within the bold sector indicates the model domain. (right) Enlarged image of the area within the stippled rectangle in the left panel. The solid curves show the Reynolds SST averaged during the observation period with a contour interval of 0.5°C, and the broken curves show isobaths in meter.

consider that atmospheric properties (e.g., wind speeds) changing linearly in time (Figure 3) result from the passage of the high-pressure system over the course of the observation. Therefore, in the present study, the vertical cross section of the observed seawater temperature is compared with those of the atmospheric properties after the detrending of temporal variations, under the assumption that all sonde data varied in time simultaneously along the observation line because the observational area is much smaller than the synoptic scale.

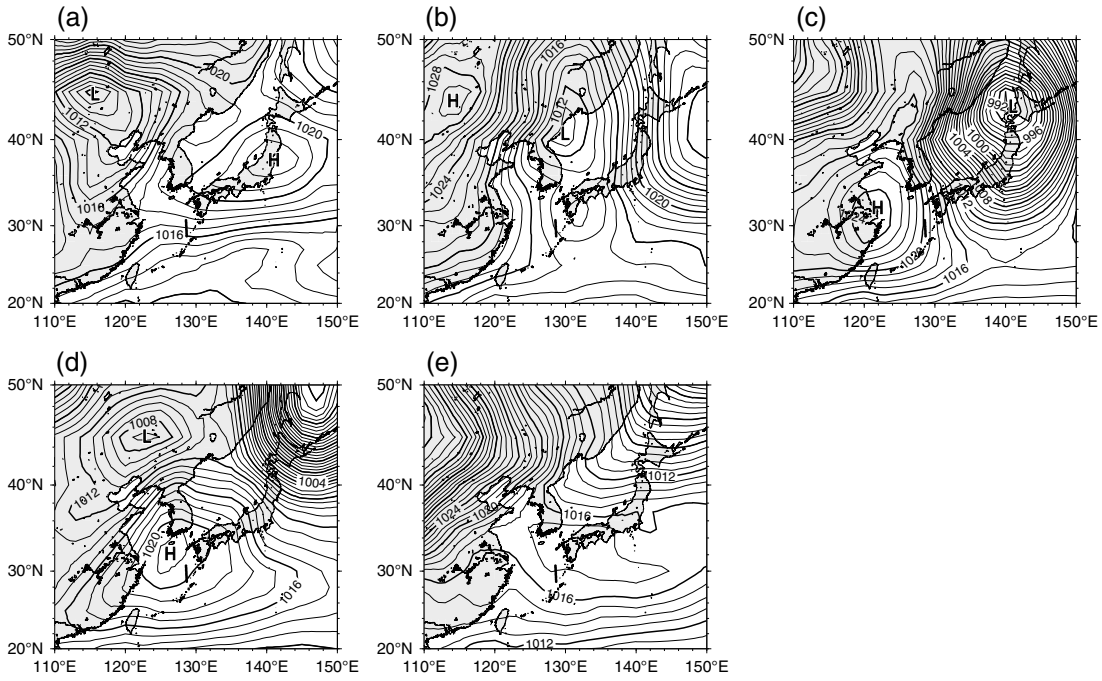

Figure 2. Horizontal distribution of the sea level pressure obtained from the NCEP reanalysis data around East Asia during the observation period on (a) 1 December 2010, (b) 2 December 2010, (c) 3 December 2010, (d) 4 December 2010, and (e) 5 December 2010. The contour interval is 1 hPa. The bold solid line represents the observation line.

©2014. American Geophysical Union. All Rights Reserved.

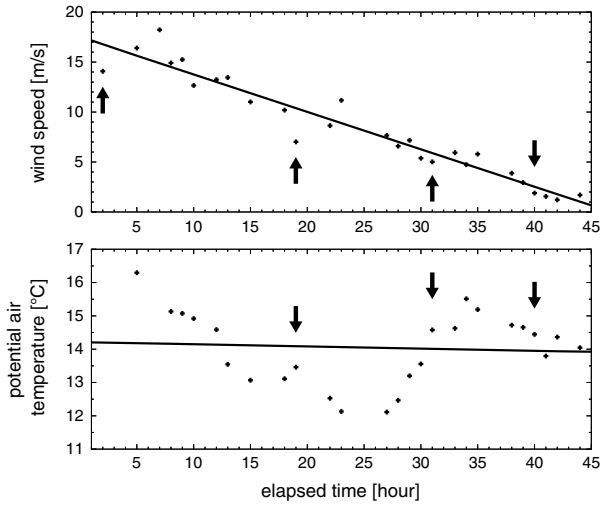

Figure 3. Time series of wind speeds (crosses, top) and potential temperature (crosses, bottom) observed by GPS sondes at 950 hPa height. The abscissa indicates the time elapsed from the start of the observations, and the ordinate indicates the wind speed and potential temperature. The solid lines show the regression line fitted to the crosses in each panel. The arrows indicate the times that observations were made at 30°N.

2.2. Gridding Procedure for XBT and GPS Sonde Data

First, observational data are gridded to depict two-dimensional cross sections of atmospheric and oceanic properties. Free-fall XBT probes are designed to descend at a speed of 1.3 m/s after deployment from research vessels, and so the horizontal distance that the probes are carried by ocean currents of $O(1)$ m/s is estimated as about 250 m when a probe reaches the lower limit of the observation depth (about 760 m in the present study). This distance is negligible when compared with station intervals (about 15 km) of the present survey, and we can thus easily map seawater temperature on a two-dimensional cross section (a latitude-depth cross section in this case) parallel to the observation line by assuming that the XBT probes measured seawater temperature vertically downward at each station. Thereafter, using a box average, the seawater temperature is gridded in boxes with horizontal length of 15 km (equal to the station interval) and vertical resolution of 10 m.

However, difficulty arises from the positioning of multiple GPS sondes released at stations separated by short intervals. It takes a few hours for each sonde to reach the tropopause (at an altitude of about 11 km), and so winds travelling at 30 m/s (a typical value beyond the 500 hPa altitude in the present case) carry the sondes downwind from each release point by more than 100 km, which is a distance much longer than the station interval of 15 km. In addition, wind speeds and directions varying stochastically in both space and time are likely to make the sonde motion complex. In fact, the trajectories of GPS sondes in both latitude-altitude and longitude-altitude spaces (Figure 4) indicate that the sondes moved eastward suddenly above the 500 hPa altitude. Hence, it is a difficult task to determine the positions of GPS sondes appropriately on a two-dimensional (horizontal position and altitude) cross section. We therefore use GPS sonde data only below the 500 hPa altitude, so as to minimize errors in determining sonde positions on the cross section. In addition, we assume that sonde motion (and hence the change in atmospheric properties) perpendicular to the observation track is relatively small because of the small displacement of sondes beneath 500 hPa (see Figure 4, right). Hence, each sonde position is projected orthogonally onto the two-dimensional (horizontal position and altitude) cross section along the observation line.

As an example, the gridding procedures for wind speeds are presented in Figures 5a–5d, where the elapsed time from the beginning of the observation (2130 UTC on 2 December) is used for the abscissa instead of the location. First, all the sonde data are projected orthogonally onto the cross section (Figure 5a). Second, the actual observation data are gridded with a resolution of 1 h in time and 10 hPa in altitude (Figure 5b) using a box average. Third, missing values are filled by horizontal spline interpolation (Figure 5c). Fourth, a linear trend of the GPS sonde data is removed at each isobaric surface to remove the synoptic-scale transition (Figure 5d). The above gridding is also conducted for air temperature and relative humidity in the same manner as for wind speed. It may be possible that the original sonde data are overly smoothed by the spline

©2014. American Geophysical Union. All Rights Reserved.

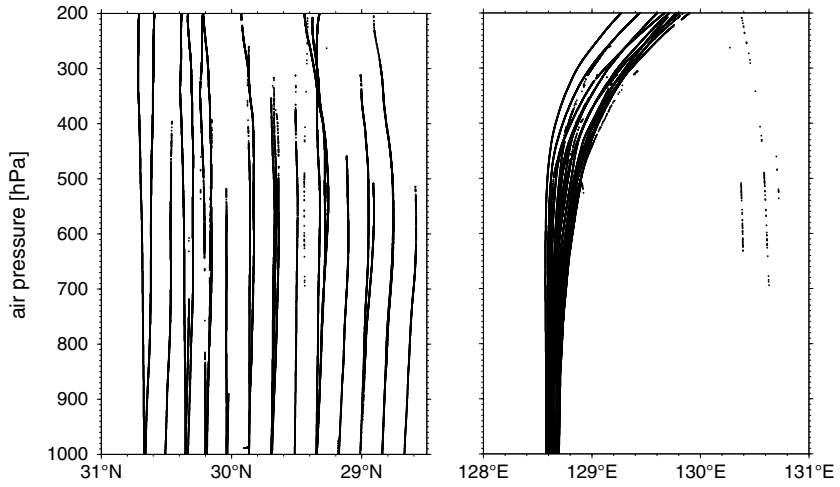

Figure 4. Positions (dots) of GPS sondes in (left) latitude-altitude and (right) longitude-altitude cross sections.

interpolation, but these interpolated data are used in this study to compute the linear trend and thus remove synoptic-scale transition.

2.3. Setup of a Regional Atmospheric Model

To interpret the results of the simultaneous XBT/GPS sonde observations, we use a regional atmospheric model, the Mesoscale Model version 3 (MM5V3) [*Grell et al.*, 1995], in a domain from 116°E to 140°E in longitude and from 21°N to 39°N in latitude (Figure 1). The horizontal grid spacing is 10 km, and there are 23 sigma levels (five levels within the mixed layer (<850 hPa)) in the vertical. The analysis data from the NCEP four-time-daily analysis product (http://dss.ucar.edu/datasets/ds083.2/) are used for initial and lateral boundary conditions. The daily Reynolds SST [*Reynolds et al.*, 2007] with horizontal resolution of 0.25° is given

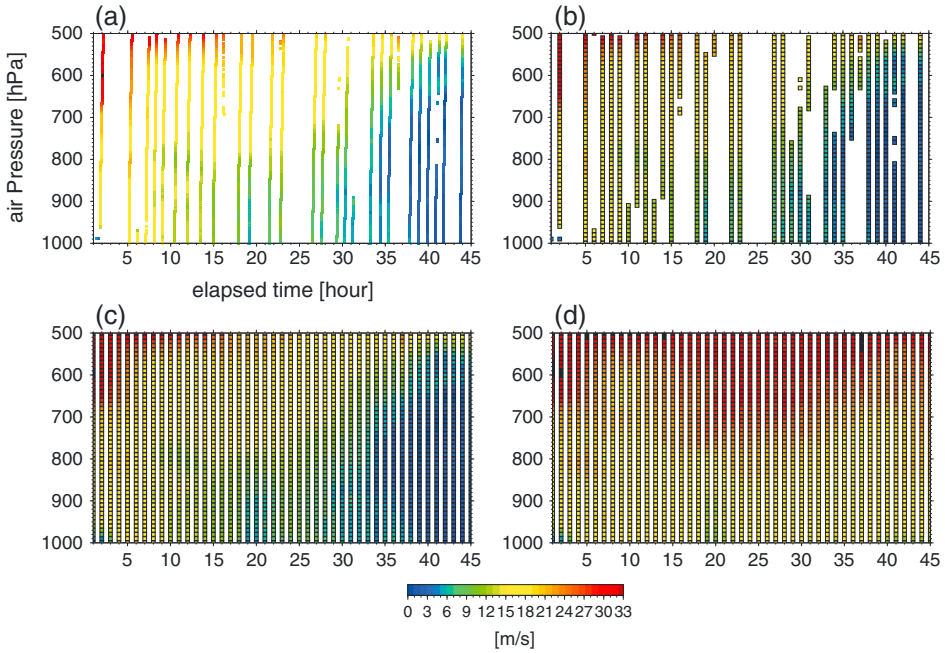

Figure 5. Vertical distribution of wind speeds obtained by GPS sondes. The abscissa shows the elapsed time from the beginning of the observation, and the ordinate shows the observation height expressed by the air pressure. (a) The actual observation data, (b) the gridded data with a resolution of 1 h in time and 10 hPa in height, (c) the interpolated data obtained by spline interpolation, and (d) the detrended data obtained by removing regression lines at each isobaric surface.

©2014. American Geophysical Union. All Rights Reserved.

at the lower boundary of the MM5V3 by interpolating linearly in time at each time step. Land surface temperature is predicted using a five-layer soil model based on the vertical diffusion equation (ISOIL = 1 in the MM5 user's guide, National Center for Atmospheric Research (NCAR) 2005). The Grell cumulus parameterization (ICUPA = 3), medium-range forecast planetary boundary layer (IBLTYP = 5), cloud and rainwater (IMPHYS = 2), and cloud radiation (IFRAD = 2) schemes are also included in the model. The radiative condition is chosen (IFUPR = 1) for the upper boundary (100 hPa level) to absorb upward propagating wave momentum. The above choices of model settings are optimal in modeling the atmospheric processes over the East Asian marginal seas (e.g., development of extratropical cyclones [*Yamamoto and Hirose*, 2007; *Isobe and Kako*, 2012]).

In the present study, we seek modeled cross sections of atmospheric properties (potential temperature and wind speed) similar to those observed above the actual Kuroshio front in December 2010, regardless of the periods of the computation. This is because the sharpness and locations of the Kuroshio front are not always well reproduced by the synthesis of satellite-derived SSTs especially in the cloudy East China Sea during winter, as shown later in Figure 8, where SST, observed using XBTs, is compared with the Reynolds SST. To model the atmospheric properties above a realistic Kuroshio front similar to the observed one, segmented integrations are carried out 9 times in the time course of November to February 2002 to 2011 (36 months in total). The obtained properties provide a modeled result appropriate for investigating processes that actually occurred from 2 to 4 December 2010.

3. Results of Simultaneous XBT/GPS Sonde Observations

3.1. Cross Sections of Oceanic and Atmospheric Properties in Each Survey

Figures 6a–6e shows cross-sectional views of potential temperature, humidity, wind speed, and seawater temperature along with wind vectors averaged below the 950 hPa level. Note that the abscissa indicates latitudes (north (left)-south (right)) along the observation line, not the elapsed time as in Figure 5, using the navigation record during the surveys. A box average with a horizontal length of 15 km (equal to the station interval) and vertical length of 10 hPa is applied to an interpolated data set such as the wind speed in Figure 5. We carried out a four-time survey over 44.5 h, and four cross-sections were thus obtained in total.

First, let us note the seawater temperature observed using XBTs. It is clear that the observation line certainly crosses the Kuroshio front around 29.5°N–30°N (Figure 6d), which is consistent with the front location revealed by the Reynolds SST (see Figure 1). The ocean currents just at the Kuroshio front are strongest among those in the observed area, and so warm water carried from the southwest is found in the frontal region. In addition, an oceanic mixed layer prevails above the 100 m depth, suggesting that the upper ocean is strongly affected by the atmosphere.

It is interesting that the cross sections of the potential temperature (Figure 6a) in the atmosphere reveal the development of an atmospheric mixed layer below the 900 hPa level, suggesting that the oceanic influence also prevails in the lower troposphere above the Kuroshio front. As shown in isobaric maps in Figure 2, the northerly winds prevail at the beginning of the observation (2 and 3 December; Figures 2b and 2c and Figure 6e), and a high-pressure system with moderate winds occupies the East China Sea afterward (Figures 2d and 6e). Hence, a cool air mass occupies the atmospheric mixed layer from 0600 UTC on 3 December to 0300 UTC on 4 December (Figure 6a). Thereafter, the mixed layer gradually warms, probably owing to the warm Kuroshio water beneath it. The cool air mass saturates the atmospheric mixed layer at the top of the layer (900 hPa level in Figure 6b).

The effect of the Kuroshio on the atmospheric processes is visible in the wind field (Figure 6c), as well as the temperature and humidity. Overall, the wind speeds in the mixed layer are lower than those above the 800–260 hPa level because of the friction effect in the atmospheric boundary layer; note that the Kuroshio Current at the shelf break ($O(1)$ m/s [*Isobe*, 2008]) is 1 order of magnitude slower than the winds ($O(10)$ m/s; Figure 6e). Of particular interest is that the wind speeds do not strengthen above the warm Kuroshio water, as shown by previous studies based on satellite data analyses, but rather weaken locally above the Kuroshio front in snapshots obtained by in situ GPS sonde/XBT observations. This local weakening of the surface wind is always found near 30°N (see arrows in Figure 6c), collocated with the Kuroshio front (Figure 6d). This locality is also suggested even in the original sonde data set before interpolating and detrending, although synoptic scale motion makes its identification unclear. Figure 3 shows that the local

©2014. American Geophysical Union. All Rights Reserved.

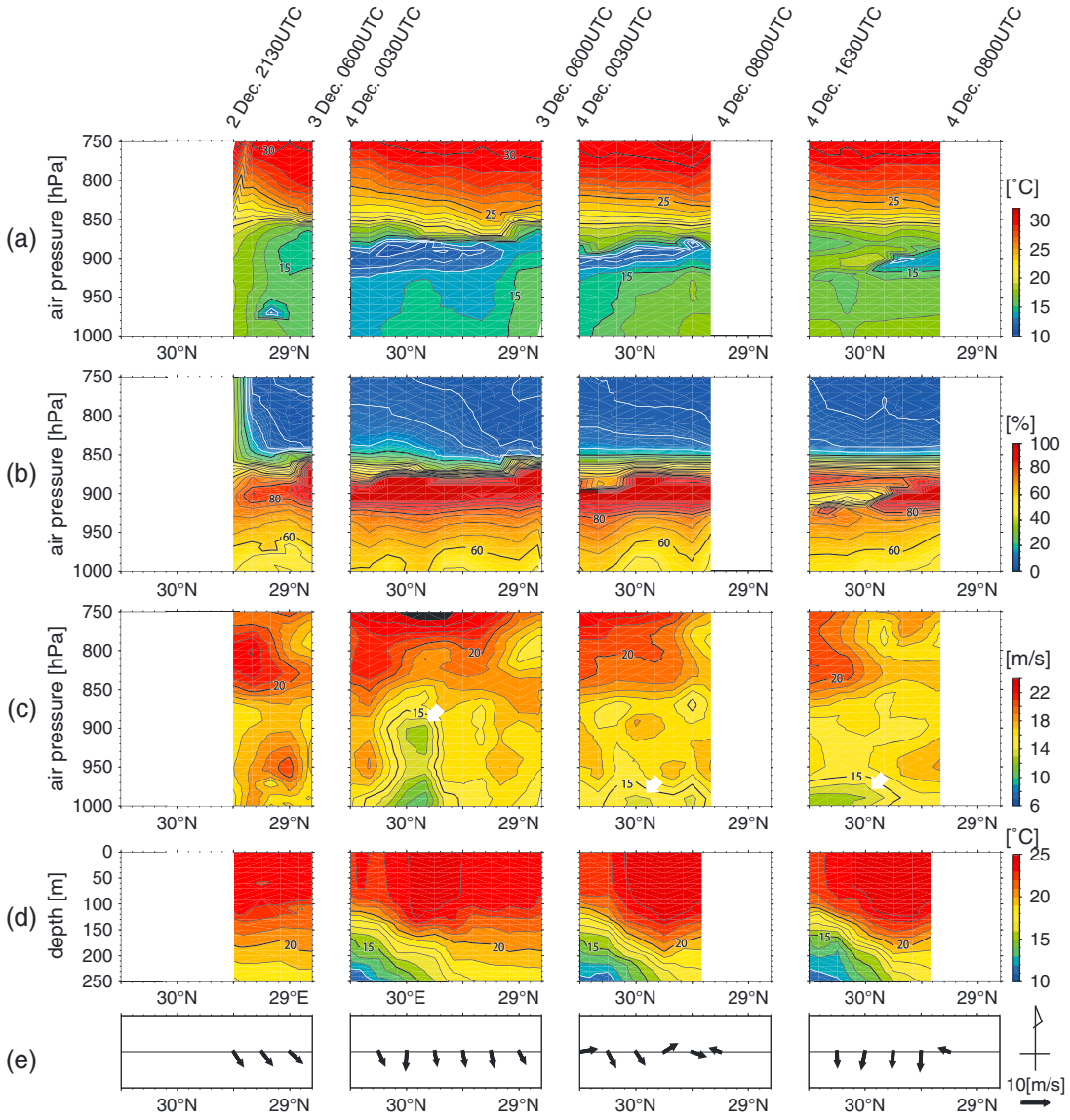

Figure 6. Cross sections of (a) potential temperature, (b) relative humidity, (c) wind speed, (d) seawater temperature, and (e) surface wind vectors along the observation line. The abscissa indicates the latitude, and the ordinate indicates the height expressed by the air pressure in Figures 6a–6c and ocean depth in Figure 6d, respectively. Surface wind vectors in the direction to which the winds blow are averaged from the lowest observation height to 950 hPa. The contour intervals in Figures 6a, 6b, 6c, and 6d are 1°C, 5%, 1 m/s, and 1°C, respectively. The white arrows in Figure 6c are used for pointing out the areas where winds weaken above the Kuroshio front. The wind vectors are depicted once every 0.25° because of overcrowding.

weakening of the wind speed and the warming of potential temperature are found at times when the observation is made at 30°N (the arrows). However, it should be noted that the weakening of the surface winds varies in observational time, suggesting that the phenomenon is relatively unstable in time. The linear trend related to the passing of the synoptic event has been removed from the GPS sonde data, and this local weakening is thus regarded as an atmospheric response generated above the local oceanic structure of the Kuroshio front.

3.2. Averaged Field Over the Course of the Observation

The relationship between atmospheric and oceanic properties is well demonstrated by averaging all the observed cross sections to smoothen the variability found in each survey. Figure 7 shows cross sections of seawater temperature, potential air temperature, humidity, and wind speed averaged over the four-time surveys. Compared with the case in Figure 6a, it is more evident that potential air temperature increases just above the mainstream of the Kuroshio Current, where SST is highest (Figure 7a). This suggests that warm

©2014. American Geophysical Union. All Rights Reserved.

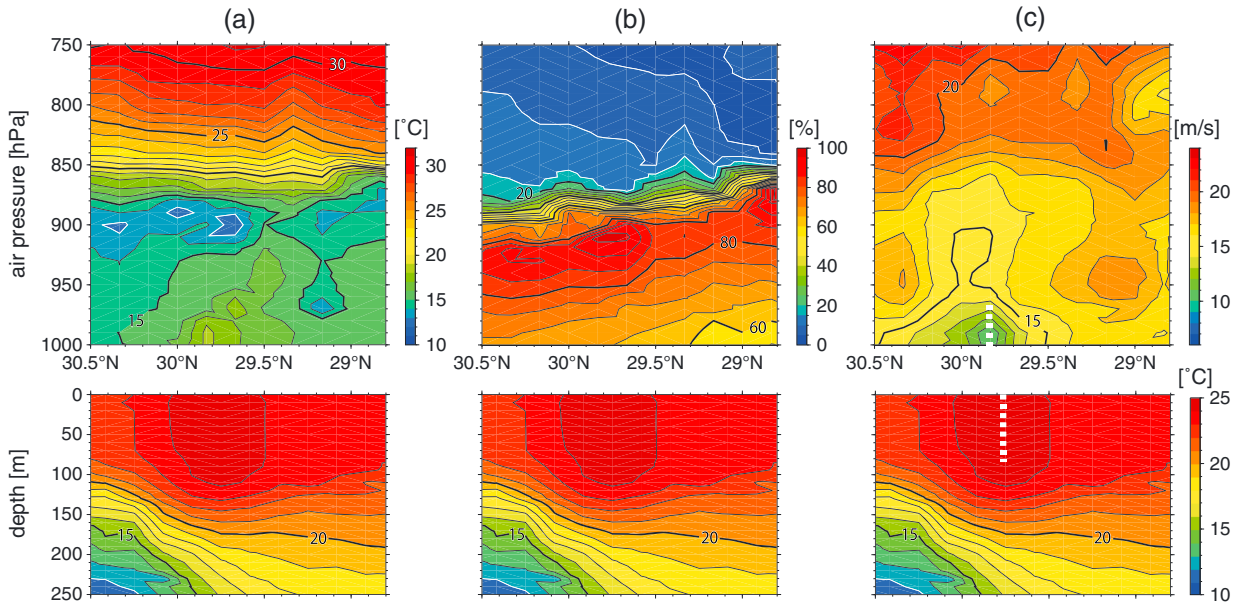

Figure 7. Cross sections of the averages of the XBT and GPS sonde observation data shown in Figure 6. The cross sections of (a) potential air temperature, (b) relative humidity, (c) and wind speed are averaged for the 44.5 h survey using the GPS sondes. (bottom row) Also shown are the same cross sections of seawater temperature averaged using all the XBT data. The abscissa indicates the location along the observation line, and the ordinates indicate (top row) the height expressed by the air pressure and (bottom row) the ocean depth expressed in meters. Figures 7a–7c show the contour intervals of air potential temperature, relative humidity, and wind speeds which are 1°C, 5%, and 1 m/s, respectively, and the interval of seawater temperature is 1°C. The white dotted lines in Figure 7c indicate the cores (positions of the maximal value) of weakening winds and warm seawater.

Kuroshio water supplies heat to the low-level atmosphere, so that the atmospheric boundary layer is likely to develop owing to convective instability. It is also noted that the air temperature increases by up to 4 K from 30.5°N to 29.8°N. In addition, both potential air temperature and humidity demonstrate that the height of the mixed layer increases up to 900 hPa as we go to the south (Figures 7a and 7b). As shown in Figure 6e, northwesterly and northerly winds normal to the Kuroshio front prevail at the beginning of the observation, and it is thus considered that the vertical transfer of heat, water vapor, and momentum develops gradually as the cool and dry air mass carried by these winds moves over the Kuroshio water.

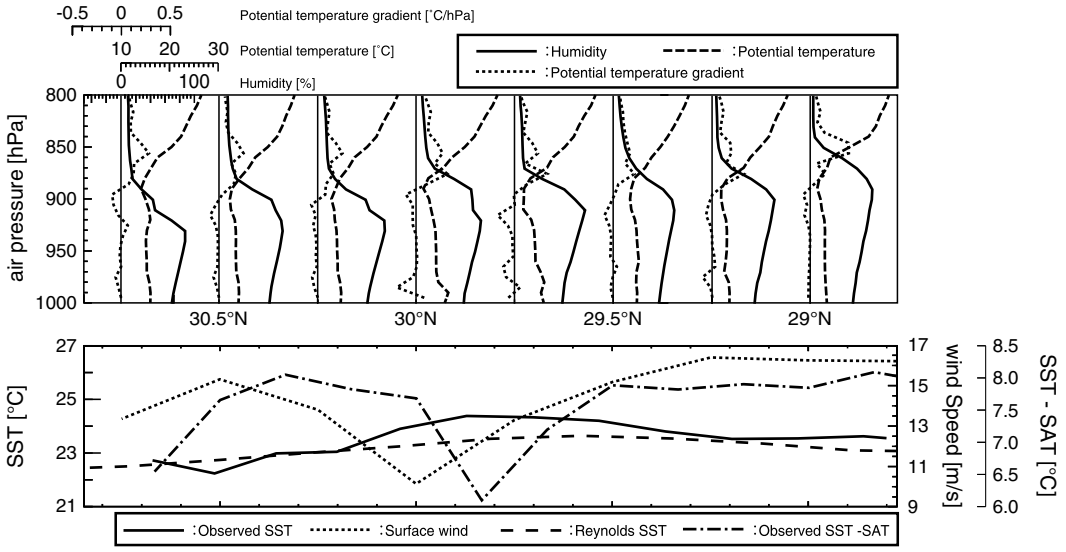

Figure 8. Comparison between data recorded by GPS sondes and XBTs at selected positions along the observation line (abscissa). (top row) The vertical profiles of relative humidity, potential air temperature, and vertical gradient of the potential temperature with solid, broken, and dotted curves, respectively. (bottom row) The observed SST in the present survey (solid line), surface wind speed (dotted line), Reynolds SST (broken line), and the observed SST minus surface air temperature (dash-dotted line) along the observation line.

©2014. American Geophysical Union. All Rights Reserved.

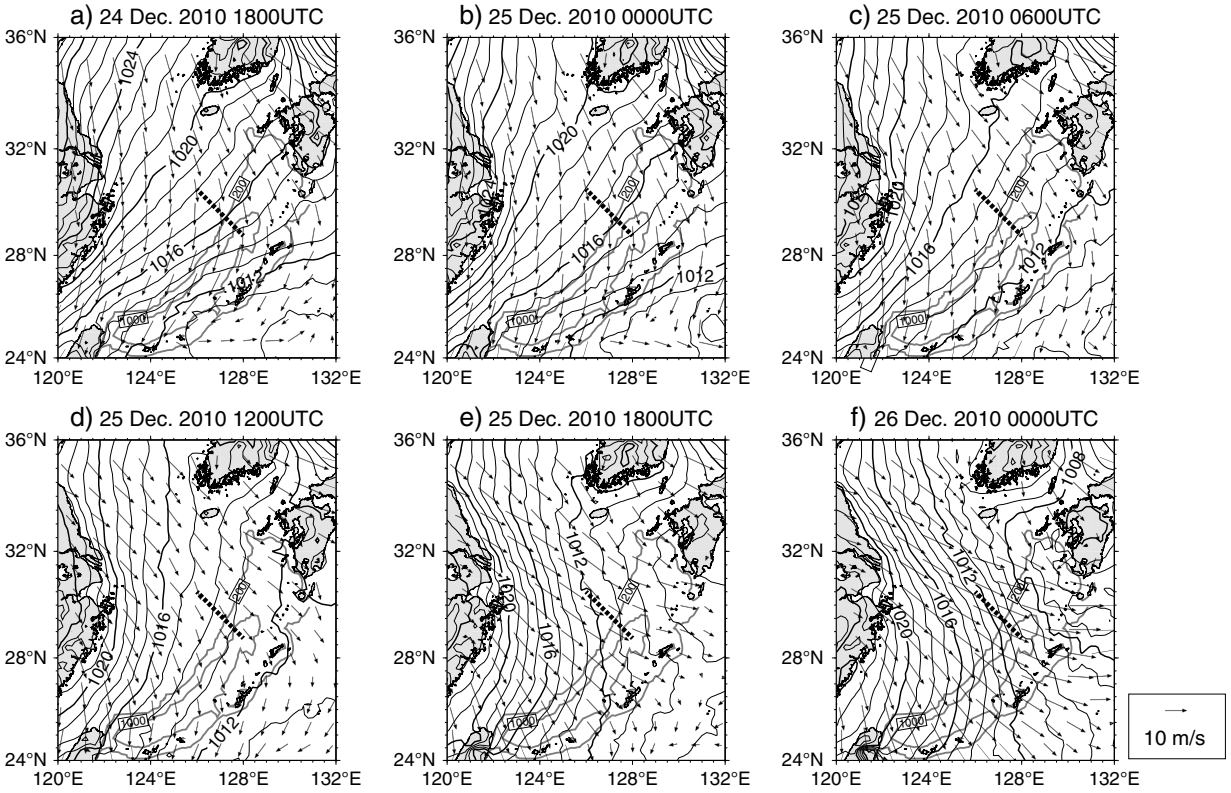

Figure 9. Horizontal distribution of the sea level pressure (solid curves) and wind vectors computed by the MM5V3 during the period 1800 UTC on 24 December 2010 through 0000 UTC on 26 December 2010. The cross sections in Figure 10 are depicted along the bold broken line shown in this figure. The isobaths expressed in meter are also drawn as the gray curves. The contour interval of the sea level pressure is 1 hPa, and the reference of wind vectors is shown at the right in Figure 9f. The wind vectors are plotted once every 10 grids for clarity.

Although the wind intensification above warm oceans due to the vertical momentum transfer has been pointed out in previous studies, the finding in the present surveys is that the surface winds over the Kuroshio front are weaker than surrounding winds (Figure 7c). It should be noted that the location where the surface winds weaken is not just above the center of the seawater warm-core (29.7–29.8°N), but is shifted to the northern flank (29.8–29.9°N).

The above relationship between atmospheric and oceanic properties averaged over the surveys is well illustrated in Figure 8 with graphs of potential air temperature, relative humidity, and vertical gradient of the potential temperature below the 800 hPa level together with the surface wind speed (at 950 hPa), observed SST, and observed SST minus surface air temperature (SAT at 1000 hPa). The oceanic effect is well revealed as the weakening of the wind at the northern flank of the Kuroshio frontal area, which is not the peak of seawater temperature but the peak of its horizontal gradient (Figure 8, bottom). Figure 8 (top) clearly shows that the top of the atmospheric mixed layer where the relative humidity is saturated rises as we go southward, and Figure 8 (bottom) shows that the lower atmosphere is definitely heated because SST is always higher than SAT. This result suggests that the heat and water vapor supplied by the Kuroshio to the atmosphere deepen the atmospheric mixed layer gradually as the cool and dry air mass from the winter Asian landmass moves southeastward (leeward, see wind vectors in Figure 6e) over the Kuroshio Current.

4. Discussion

4.1. Possible Weakening Process of Surface Winds Above the Kuroshio Front

The observed atmospheric and oceanic properties provide us with a plausible scenario for the local weakening of surface winds, and not the local intensification as reported by previous studies, at the northern flank of the Kuroshio front. The aforementioned deepening of the atmospheric mixed layer suggests that surface wind speeds are affected by the vertical momentum transfer associated with the convection driven by the heat supply from warm water [*Wallace et al.*, 1989]. Especially at the beginning of the observation, the intense

©2014. American Geophysical Union. All Rights Reserved.

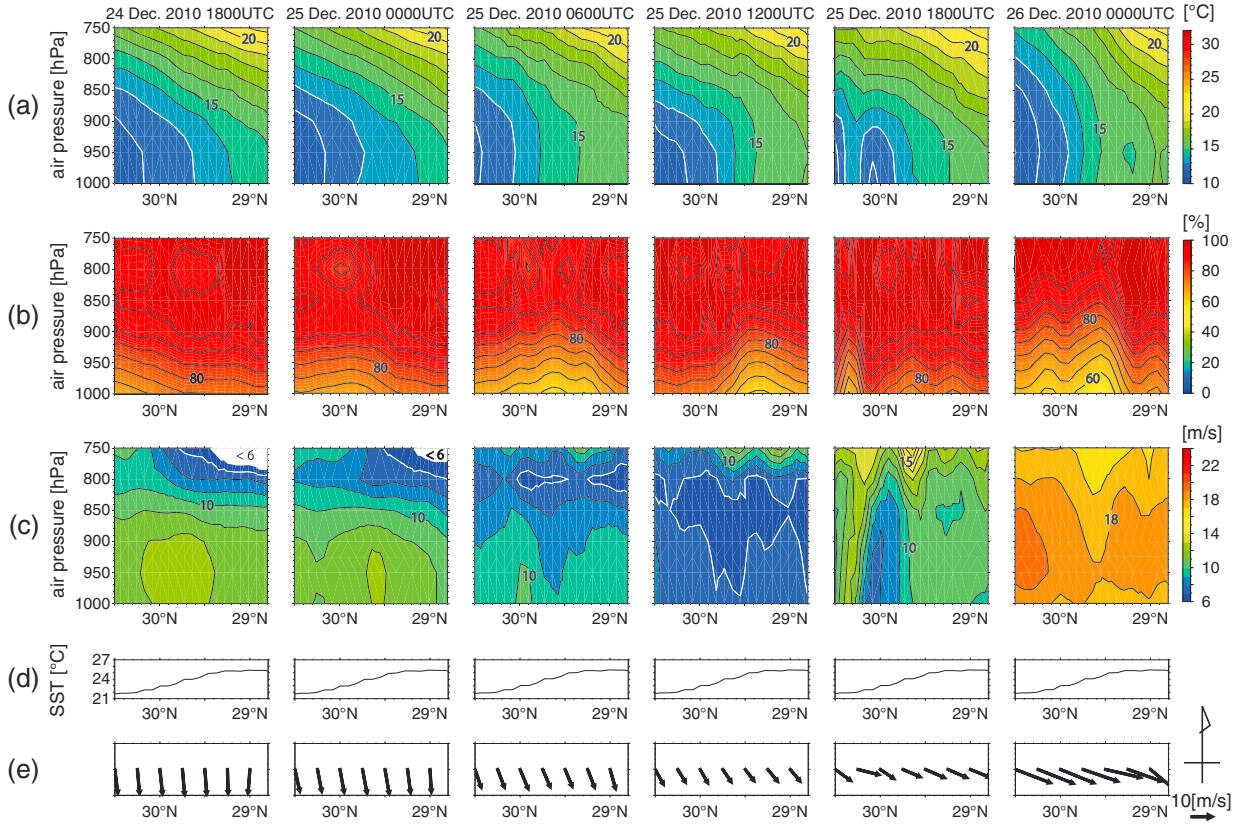

Figure 10. Cross sections of (a) potential temperature, (b) relative humidity and (c) wind speed, (d) horizontal distribution of SST, and (e) surface wind vectors in the direction to which winds blow in the MM5V3 during the period 1800 UTC on 24 December 2010 through 0000 UTC on 26 December 2010 along the bold broken line in Figure 9. Note that Figures 10a, 10b, 10c, and 10e are all modeled results, while Figure 10d is derived from the Reynolds SST imposed on the MM5V3 at the lower boundary. The wind vectors at 1000 hPa are depicted once every 0.25° in Figure 10e. The abscissa shows latitudes along the broken line in Figure 9. The ordinates indicate heights expressed by the air pressure in Figures 10a, 10b, and 10c and potential temperature in Figure 10d. The contour intervals in Figures 10a, 10b, and 10c are 1°C, 5%, and 1 m/s, respectively.

northwesterly or northerly winds prevail over the Kuroshio front (2–3 December; Figure 6e). These cold and dry winds from the winter landmass are associated with a pressure pattern moving eastward with a high- (low-) pressure system west (east) of the East China Sea (Figure 2). Once the cold air mass flows into the lower atmosphere over the warm Kuroshio water, the stratification becomes stable (unstable) above (beneath) the air mass owing to the suppression (intensification) of the convective instability. It is therefore considered that the vertical mixing of momentum prevails only below the altitude to which the cold air mass flows (up to 900 hPa in observation, see the maximal vertical gradient of potential temperature between 850 and 900 hPa in Figure 8 (top)). The atmospheric mixed layer must be shallow at the northern flank of the Kuroshio front when cool air masses come from the north or northwest as shown in Figures 7a and 7b. Thereafter, the mixed layer becomes deep as we go leeward (southward or southeastward, see Figure 8 (top) in which the coldest and saturated air mass is located higher in the south, presumably because the heat and the water vapor are supplied intensively from the Kuroshio water as the air mass moves leeward). In this case, the oceanic "nonslip" condition decelerates the northerly or northwesterly winds within the shallow mixed layer that is insufficiently developed at the northern flank of the Kuroshio front (Figure 7c). This seems to be reasonable because weakening winds isolated from surroundings are unlikely to have a "source" except for the nonslippery sea surface. Thereafter, the surface wind speed increases gradually as the mixed layer deepens southward, because the deceleration due to the nonslippery sea surface in the relatively deep mixed layer becomes less effective than that in the shallow mixed layer and because the surface winds are gradually accelerated by the momentum mixing with strong winds aloft. On the cool continental side of the Kuroshio front, the winds in the mixed layer (about 950 hPa) remain strong because of the absence of the intense vertical momentum transfer.

©2014. American Geophysical Union. All Rights Reserved.

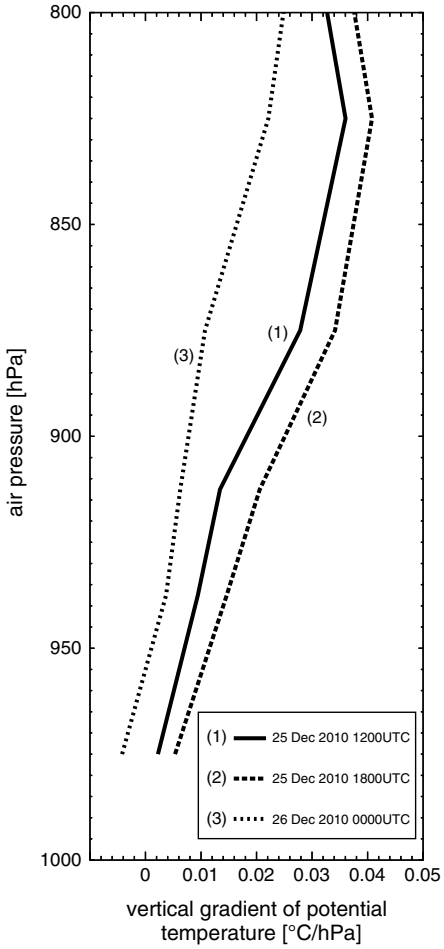

Figure 11. Vertical profile of the vertical gradient of potential temperature during the period 1200 UTC on 25 December 2010 through 0000 UTC on 26 December 2010. The times for each line are shown by each profile.

The weakening of surface winds locally above oceanic fronts has rarely been reported in previous studies in spite of a relatively fine resolution of a satellite scatterometer (~25 km) sufficient for observing the local weakening of surface winds (with core width of about 50 km (Figure 7c)). In addition, the weakening is never seen in long-term averaged maps based on satellite observations [e.g., *Chelton et al.*, 2001]. A plausible answer is that the weakening of surface winds over oceanic fronts occurs as a transient state with a relatively short duration. Certainly, the present observation was conducted just at the onset of the northerly and northwesterly winds, which might trigger the local weakening of the surface winds. To confirm the process that generates the local and probably transient weakening of the surface winds at the northern flank of the Kuroshio front, numerical modeling is next conducted using a regional atmospheric circulation model.

4.2. Spatiotemporal Scales of the Local Weakening of Surface Winds

In investigating the weakening of the surface winds at the northern flank of the Kuroshio front using the MM5V3, we first seek periods appropriate for analyzing model results. This is because, as we suggested above, two requirements should be satisfied to reproduce the local weakening of the surface winds, and they are not always met by the conditions of the model. The first is the onset of the cold and dry winds blowing from the colder side of the Kuroshio front (northwesterly winds in this case). The second is that, at the lower boundary, the Kuroshio front needs to be sufficiently sharp to "anchor" the local weakening of the winds at the northern flank. In the observed case, the sharpness of the Kuroshio front is 5.0×10^{-5}°C/m, but the Reynolds SST (Figure 8, bottom) has sharpness of 1.0×10^{-5}°C/m. However, SSTs synthesized from multiple satellite observations (Reynolds SST in the present study) are not always accurate, especially in the cloudy East China Sea during winter. In fact, the sharpness of the Kuroshio front revealed by the Reynolds SST is much weaker than that observed directly using XBTs on 2–4 December 2010 (Figure 8, bottom).

Figure 9 shows maps of the modeled sea level pressure and wind vectors from 1800 UTC on 24 December to 0000 UTC on 26 December 2010 (30 h in total). The reason for choosing this period from the 36 month computations is that the atmospheric and oceanic circumstances in the model are closest to those observed in the actual ocean during this period. In total, snapshots of 76 cases (saved every 6 h) among 4320 (36 month (=25,920 h)/6 h) show conditions favorable for the weakening of wind (i.e., onset of the northwesterly winds over the sharp front); the weakening winds are found in 18 snapshots (23%), although some cases are not as remarkable as the example shown later in Figure 10. No statistical significance test to ensure this probability is performed because ambiguous cases (not included in the 18 cases) might justify our scenario for the local wind weakening. First, it can be confirmed that northwesterly winds gradually strengthen, especially in the latter half of the period as a high-pressure system over the Asian landmass extends eastward over the southern East China Sea. Second, the sharpness of the Kuroshio front as we observed on 2–4 December 2010 is reproduced in the SST imposed at the modeled sea surface (Figure 10, bottom row). We choose a cross section along the bold broken line in Figure 9 because there is remarkable weakening of the surface winds along it. Choosing the cross section, which is different from the observation line, suggests the possibility of local weakening of the surface winds anywhere over the northern flank of the Kuroshio front.

©2014. American Geophysical Union. All Rights Reserved.

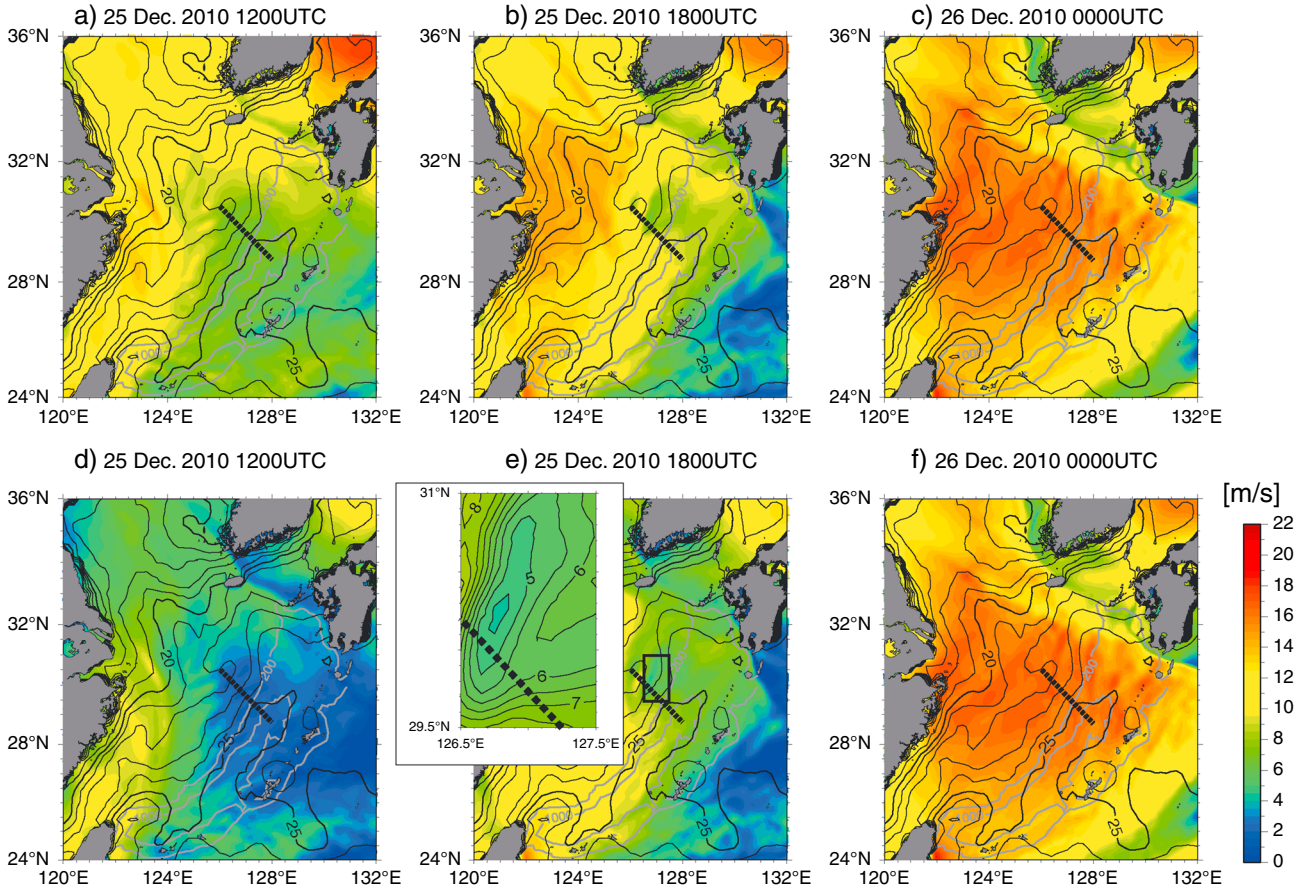

Figure 12. Horizontal distributions of wind speeds computed using the MM5V3 along with Reynolds SST during the period 1800 UTC on 24 December 2010 through 0000 UTC on 26 December 2010. (top row) Wind speed maps. (bottom row) The same maps but with the removal of a horizontal plane fitted by a least squares method. The cross sections in Figure 10 are depicted along the broken line in this figure. The color tones show the wind speeds scaled at the right of this figure, and the solid curves indicate the SST with a contour interval of 1°C. The gray curves show isobaths of 200 and 1000 m, respectively. The (e) area within the rectangle is enlarged at the upper left in the same panel. The contour interval in this enlarged panel is 0.5 m/s.

Vertical cross sections of potential air temperature, humidity, and wind speeds along the bold broken line in Figure 9 demonstrate that the weakening of the surface winds within the atmospheric mixed layer above the Kuroshio is well reproduced in the model and that the weakening process is of short duration after the onset of the intense northwesterly winds at 1800 UTC on 25 December (Figure 10). No local weakening of the wind speeds is revealed above the Kuroshio front before this time. Rather, the surface winds strengthen slightly above the northern flank of the Kuroshio front (29.5°N–30°N) at 1800 UTC on 24 December and 0000 UTC on 25 December, when the northerly or northeasterly (along-front) winds prevail over the shelf break of the East China Sea (Figures 9a and 9b). Thereafter, the northwesterly (cross-front) winds strengthen (Figures 9e and 10e), and a dome-like pattern of weak wind rapidly develops over the northern flank of the Kuroshio front (30°N) at 1800 UTC on 25 December. Concurrently, a dome-like pattern is revealed in the cross section of the potential temperature at the same location. However, the modeled wind and temperature patterns (Figure 10) similar to those observed over the actual Kuroshio front (Figure 7) mostly disappear after 6 h (at 0000 UTC on 26 December) despite the continuation of the intense northwesterly winds (Figures 9f and 10e).

This short duration is due to the rapid development of the mixed layer in the low-level atmosphere. Indeed, the atmospheric mixed layer deepens over 6 h above the Kuroshio front as shown in the cross sections of potential temperature and humidity during the period 1800 UTC on 25 December through 0000 UTC on 26 December in Figure 10. In addition, the temporal variation of the vertical gradient of the potential air temperature at 30°N (Figure 11) indicates that the vertical mixing in the low-level atmosphere rapidly proceeds on a time scale of less than 6 h, which is much less than the time scale observed in the actual ocean, see Figure 6 in which the dome-like weakening of wind continued during the 44.5 h observation at least. This is

©2014. American Geophysical Union. All Rights Reserved.

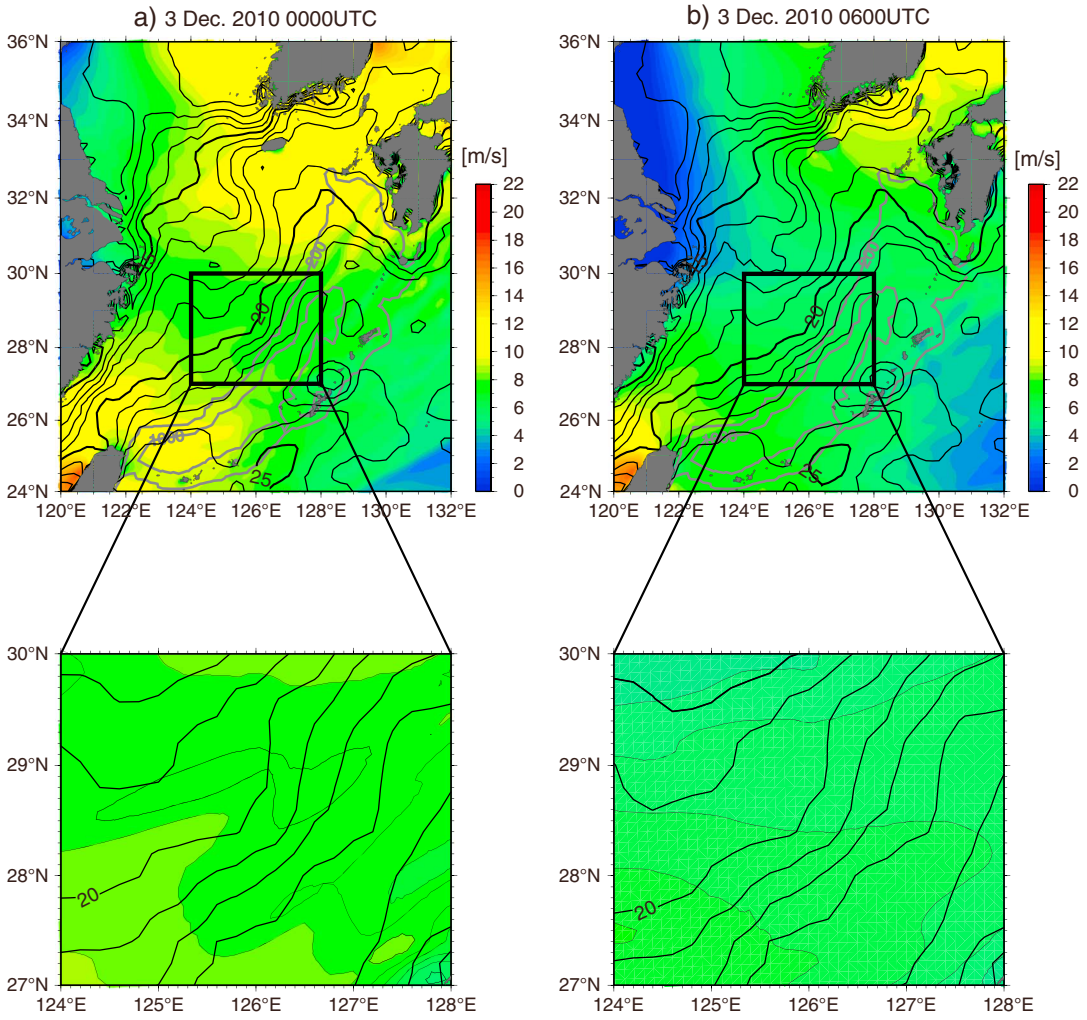

Figure 13. Horizontal distributions of wind speeds in the additional experiment (see the main text for details) at (a) 0000 UTC and (b) 0600 UTC on 3 December 2010. The areas within the rectangles in Figure 13a are enlarged in Figure 13b. The color tones show wind speeds scaled at the right of Figures 13a and 13b, and the solid curves indicate SST with a contour interval of 1°C. The gray curves show isobaths of 200 and 1000 m.

probably explained by the air mass at the top of the atmospheric mixed layer being much colder (less than 10°C, see the 900 hPa height in Figure 6a) than that modeled in the present case (~15°C) and the enhanced stratification caused by this cold air mass likely preventing the vertical mixing from developing upward beyond the mixed layer rapidly.

The numerical modeling provides us with a horizontal view of the local weakening of the surface wind. Figure 12 shows maps of the wind speeds at 1000 hPa along with the SST over the model domain during the latter three periods of Figure 9; that is, the period 1200 UTC on 25 December through 0000 UTC on 26 December 2010 (Figure 12, top row). To emphasize the locality that might appear in the wind field, also shown are the same maps but with the removal of a horizontal plane fitted to the two-dimensional wind speed field by a least squares method (Figure 12, bottom row). In Figure 12 (top row), the wind speed gradually increases above the Kuroshio over the course of 12 h. During this intensification of the surface wind, a domain with low wind speeds forms locally from 126.5°E to 127.5°E in longitude and from 30°N to 31°N in latitude (see the inset map of Figure 12e), at 1800 UTC on 25 December. However, it should be noted that the area where the surface winds weaken is quite narrow (100 km in length in the along-shelf direction and 20 km in width in the cross-shelf direction) and vanishes completely at 0000 UTC on 26 December. Hence, it is concluded that the surface wind weakens either transiently in time or locally in space. This result is consistent with the fact that the weakening of the surface wind has rarely been detected by satellite observations.

©2014. American Geophysical Union. All Rights Reserved.

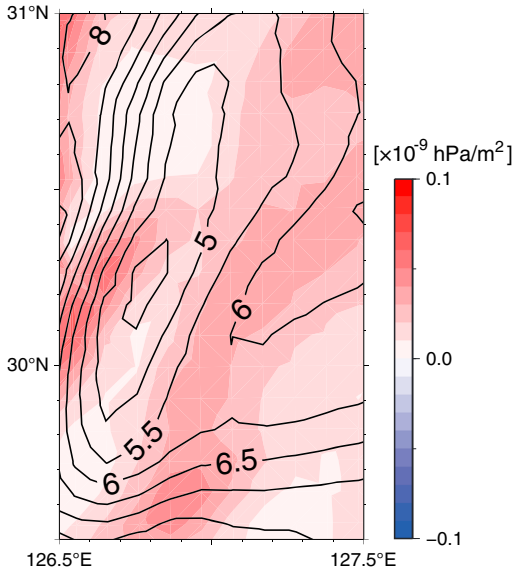

Figure 14. Horizontal distributions of Laplacian of sea level pressure indicated by color tone superimposed on the wind speed map (solid lines) in the inset of Figure 12e. The interval of the wind speed is 0.5 m/s.

The conclusion drawn above is further confirmed by an additional experiment. This experiment uses the same SST condition as that used in the foregoing experiment, but the lateral atmospheric conditions are replaced with those during the same period as the observation. Figure 13 shows horizontal views of wind speeds at 1000 hPa and SST during the period 0000 UTC through 0600 UTC on 3 December. In Figure 13a, the region of the weakening surface winds certainly appears above the area where the sharpness of the Kuroshio front is greatest (29°N, 126°E, which is different from the area that we observed). However, in contrast to the observation, the weakening vanishes completely after 6 h (Figure 13b). This is probably because the model fails to reproduce the observed cold air mass at the top of the mixed layer (data not shown), and so the vertical mixing develops beyond the mixed layer immediately after the onset of the northwesterly winds.

Nevertheless, one may consider that the weakening surface winds are caused by the sea level pressure adjustment [*Lindzen and Nigam*, 1987] rather than the vertical "nonslip condition" transfer. Figure 14 shows the horizontal distribution of Laplacian of sea level pressure superimposed on the wind speed within the area of the inset map of Figure 12e. Apparently, the Laplacian of the surface pressure is not consistent with the wind speed pattern. Therefore, it is considered that the adjustment of sea level pressure does not contribute to the weakening of surface winds, at least during the study period.

5. Summary

A field measurement using XBTs and GPS sondes simultaneously was conducted across the Kuroshio front at the shelf break of the winter East China Sea to map seawater temperature and atmospheric properties (air temperature, humidity, and wind speed) on a single vertical two-dimensional plane. This survey demonstrates that the surface winds weaken, not strengthen as reported by previous studies, locally at the northern flank of the Kuroshio front. Our conclusions are summarized schematically in Figure 15. A plausible scenario suggested on the basis of the observed data in conjunction with regional atmospheric numerical modeling follows. First, as a high-pressure system moves eastward from the Asian landmass, intense and cool northwesterly winds start to prevail over the Kuroshio front. A cold air mass carried by the northwesterly winds isolates the atmospheric boundary layer from higher layers with intense winds owing to the suppression of vertical momentum mixing aloft. Therefore, the vertical heat and momentum transfers induced by warm Kuroshio water are restricted within the atmospheric mixed layer developed in the lower atmosphere. Furthermore, the mixed layer deepens gradually as we move

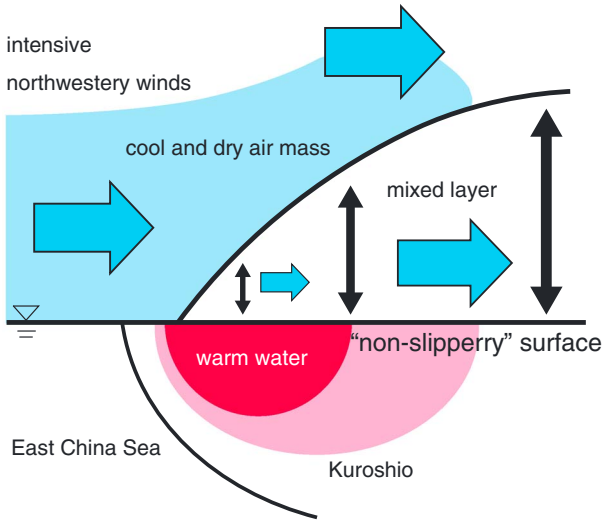

Figure 15. Schematic view of the mechanism for local and transient weakening of wind speed over the northern flank of the Kuroshio front in the winter East China Sea. The atmospheric and oceanic vertical section is viewed from the southwest to the northeast. The change in wind speed is expressed by the size of the blue arrows.

©2014. American Geophysical Union. All Rights Reserved.

leeward under the northwesterly winds normal to the Kuroshio front, while the mixed layer is relatively shallow in the early stage of its development at the northern flank of the Kuroshio front. As a result, it is considered that the nonslip condition at the sea surface locally weakens the surface winds within the relatively shallow mixed layer at the northern flank of the Kuroshio front.

It is considered that the rapid development of the atmospheric mixed layer, which is triggered by the onset of northwesterly winds over warm Kuroshio water and conveys a nonslip condition at the sea surface upward, is required for the surface wind to weaken in the atmospheric mixed layer. As the mixed layer grows under the cool northwesterly winds, the weakening of the winds becomes unclear even at the northern flank of the Kuroshio front. The mixed layer is unlikely to rapidly develop over the cold continental shelf during winter. The occurrence of the local weakening at the northern flank of the Kuroshio front may contradict previous studies using satellite data that have pointed out the local intensification of surface winds. However, taking a numerical model approach, it is found that the local weakening occurs transiently only at the onset of northwesterly winds in winter. Nonetheless, what we emphasize in the present study is that active responses of the low-level atmosphere to the Kuroshio are likely to vary more than we might have imagined.

Acknowledgments

This work is supported by a Grant-in-Aid for Scientific Research (#22244057), the Japan Society for the Promotion of Science through a Grant-in-Aid for Scientific Research (#22106002), and the Global Environment Research Fund (B-1007).

References

Chelton, D. B., S. K. Esbensen, M. G. Schalax, N. Thum, M. H. Freilich, F. J. Wintz, C. L. Gentemann, M. J. McPhaden, and P. S. Schopf (2001), Observations of coupling between surface wind stress and sea surface temperature in the eastern tropical Pacific, *J. Clim.*, *14*, 1479–1498.

Chelton, D. B., M. G. Schlax, M. H. Freilich, and R. F. Milliff (2004), Satellite measurements reveal persistent small-scale features in ocean winds, *Science*, *303*, 978–983.

Grell, G. A., J. Dudhia, and D. R. Stauffer (1995), A description of the fifth-generation Penn State/NCAR Mesoscale Model (MM5), *NCAR Tech Note* TN-398 + STR, 122pp.

Isobe, A. (2008), Recent advances in ocean-circulation research on the Yellow Sea and East China Sea shelves, *J. Oceanogr.*, *64*, 569–584.

Isobe, A., and S. Kako (2012), A role of the Yellow and East China Seas in the development of extratropical cyclones in winter, *J. Clim.*, *25*, 8328–8340.

Lindzen, R. S., and S. Nigam (1987), On the role of sea surface temperature gradients in forcing low-level winds and convergence in the tropics, *J. Atmos. Sci.*, *44*, 2418–2436.

Liu, W., X. Xie, P. S. Polito, S.-P. Xie, and H. Hashizume (2000), Atmospheric manifestation of tropical instability waves observed by QuickSCAT and Tropical Rain Measuring Mission, *Geophys. Res. Lett.*, *27*, 2545–2548.

Minobe, S., A. Kuwano, N. Komori, S.-P. Xie, and R. J. Small (2008), Influence of the Gulf Stream on the troposphere, *Nature*, *452*, 206–209.

Nonaka, M., and S.-P. Xie (2003), Covariations of sea surface temperature and wind over the Kuroshio and its extension: Evidence for ocean-to-atmosphere feedback, *J. Clim.*, *16*, 1404–1413.

O'Neill, L. W., D. B. Chelton, and S. K. Ebensen (2003), Observations of SST-induced perturbations of the wind stress field over the Southern Ocean on seasonal timescales, *J. Clim.*, *16*, 2340–2354.

Pan, J., X.–H. Yan, Q. Zheng, and W. T. Liu (2002), Observation of western boundary current atmospheric convergence zones using scatterometer winds, *Geophys. Res. Lett.*, *29*(17), 1832, doi:10.1029/2002GL015015.

Park, K.-A., P. C. Cornillon, and D. L. Codiga (2006), Modification of surface winds near ocean fronts: Effects of Gulf Stream rings on scatterometer (QuikSCAT, NSCAT) wind observations, *J. Geophys. Res.*, *111*, C03021, doi:10.1029/2005JC003016.

Reynolds, R. W., T. M. Smith, C. Liu, D. B. Chelton, K. S. Casey, and M. G. Schlax (2007), Daily High-Resolution-Blended analyses for sea surface temperature, *J. Clim.*, *20*, 5473–5496.

Takatama, K., S. Minobe, M. Inatsu, and R. J. Small (2012), Diagnostics for near-surface wind convergence/divergence response to the Gulf Stream in a regional atmospheric model, *Atmos. Sci. Lett.*, *13*, 16–21, doi:10.1002/asl.355.

Tokinaga, H., and S.-P. Xie (2009), Ocean tidal cooling effect on summer sea fog over the Okhotsk Sea, *J. Geophys. Res.*, *114*, D14102, doi:10.1029/2008JD011477.

Wallace, J. M., T. P. Mitchell, and C. Deser (1989), The influence of sea surface temperature on surface wind in the eastern equatorial Pacific: Seasonal and interannual variability, *J. Clim.*, *6*, 331–353.

Xie, S.-P., J. Hafner, Y. Tanimoto, W. T. Liu, H. Tokinaga, and H. Xu (2002), Bathymetric effect on the winter sea surface temperature and climate of the Yellow and East China Seas, *Geophys. Res. Lett.*, *29*, 2228, doi:10.1029/2002GL015884.

Yamamoto, M., and N. Hirose (2007), Impact of SST reanalyzed using OGCM on 6 weather simulation: A case of a developing cyclone in the Japan Sea area, *Geophys. Res. Lett.*, *34*, L05808, doi:10.1029/2006GL028386.

©2014. American Geophysical Union. All Rights Reserved.